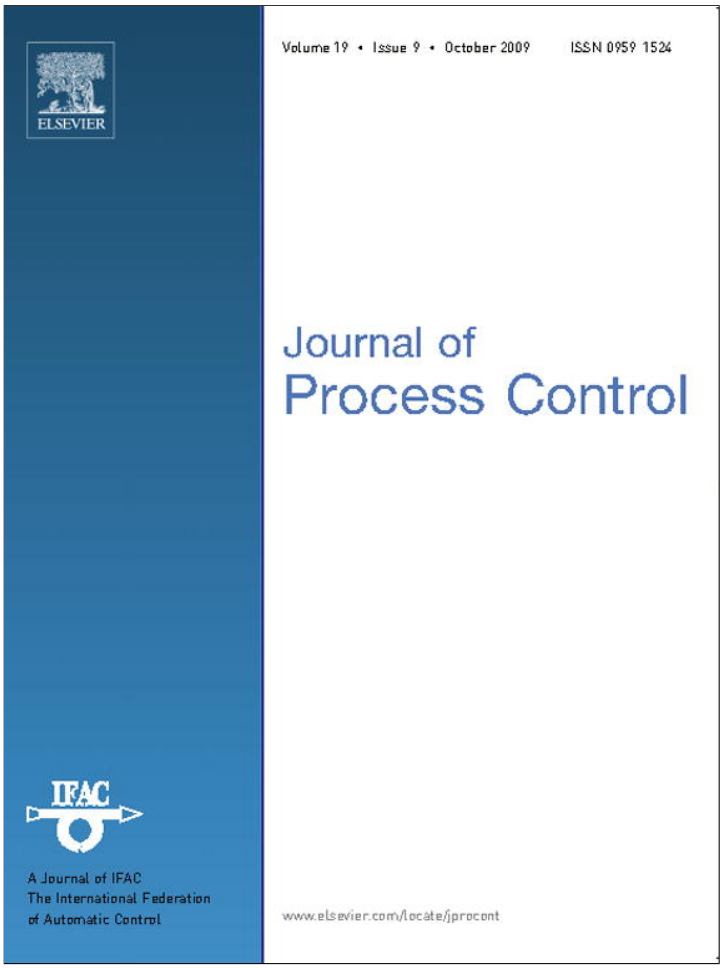

Journal of Process Control 19 (2009) 1427–1437

Contents lists available at ScienceDirect

Journal of Process Control

journal homepage: www.elsevier.com/locate/jprocont

Distributed model predictive control for plant-wide hot-rolled strip laminar cooling process

Yi Zheng [a], Shaoyuan Li [a,*], Xiaobo Wang [b]

[a] Institute of Automation, Shanghai Jiao Tong University, 800 Dong Chuan Road, Shanghai 200240, China
[b] Institute of Research and Development, Baosteel Iron and Steel Ltd. Co., 600 Fu Jin Road, Shanghai 201900, China

ARTICLE INFO

Article history:
Received 5 October 2008
Received in revised form 15 April 2009
Accepted 24 April 2009

Keywords:
Distributed model predictive control
Laminar cooling
Hot-rolled strip

ABSTRACT

Since hot-rolled strip laminar cooling (HSLC) process is a large-scale, nonlinear system, a distributed model predictive control (DMPC) framework is proposed for computational reason and enhancing the precision and flexibility of control system. The overall system is divided into several interconnected subsystems and each subsystem is controlled by local model predictive control (MPC). These local MPCs cooperate with its neighbours through the scheme of neighbourhood optimization for the improvement of global performance. The state space representation of each subsystem's prediction model is designed by finite volume method firstly, and then is linearized around the current operating point at each step to overcome the computational obstacle of nonlinear model. Moreover, since the strip temperature is measurable only at a few positions in water cooling section due to the difficult ambient conditions, an Extended Kalman Filter (EKF) is used to estimate the transient temperature of strip. Both simulation and experiment results prove the efficiency of the proposed method.

1. Introduction

Recently, customers require increasingly better quality for hot-rolled strip products, such as automotive companies expect to gain an advantage from thinner but still very strong types of steel sheeting which makes their vehicles more efficient and more environmentally compatible. In addition to the alloying elements, the cooling section is crucial for the quality of products [1]. Hot-rolled strip laminar cooling process (HSLC) is used to cool a strip from an initial temperature of roughly 820–920 °C down to a coiling temperature of roughly 400–680 °C, according to the steel grade and geometry. The mechanical properties of the corresponding strip are determined by the time–temperature-course (or cooling curve) when strip is cooled down on the run-out table [1,2]. The precise and highly flexible control of the cooling curve in the cooling section is therefore extremely important.

Most of the control methods (e.g. Smith predictor control [3], element tracking control [4], self-learning strategy [6] and adaptive control [5]) pursue the precision of coiling temperature and care less about the evolution of strip temperature. In these methods, the control problem is simplified so greatly that only the coiling temperature is controlled by the closed-loop part of the controller. However, it is necessary to regulate the whole evolution procedure of strip temperature if better properties of strip are required. This is a nonlinear, large-scale, MIMO, parameter distributed complicated system. Therefore, the problem is how to control the whole HSLC process online precisely with the size of HSLC process and the computational efforts required.

Model predictive control (MPC) is widely recognized as a practical control technology with high performance, where a control action sequence is obtained by solving, at each sampling instant, a finite horizon open-loop receding optimization problem and the first control action is applied to the process [7]. An attractive attribute of MPC technology is its ability to systematically account for process constraints. It has been successfully applied to many various linear [7–12], nonlinear [13–17] systems in the process industries and is becoming more widespread [7,10]. For large-scale and relatively fast systems, however, the on-line implementation of centralized MPC is impractical due to its excessive on-line computation demand. With the development of DCS, the field-bus technology and the communication network, centralized MPC has been gradually replaced by decentralized or distributed MPC in large-scale systems [21,22] and [24]. DMPC accounts for the interactions among subsystems. Each subsystem-based MPC in DMPC, in addition to determining the optimal current response, also generates a prediction of future subsystem behaviour. By suitably leveraging this prediction of future subsystem behaviour, the various subsystem-based MPCs can be integrated and therefore the overall system performance is improved. Thus the DMPC is a good method to control HSLC.

* Corresponding author.
E-mail address: syli@sjtu.edu.cn (S. Li).

0959-1524/$ - see front matter © 2009 Elsevier Ltd. All rights reserved.
doi:10.1016/j.jprocont.2009.04.012

Some DMPC formulations are available in the literatures [18–25]. Among them, the methods described in [18,19] are proposed for a set of decoupled subsystems, and the method described in [18] is extended in [20] recently, which handles systems with weakly interacting subsystem dynamics. For large-scale linear time-invariant (LTI) systems, a DMPC scheme is proposed in [21]. In the procedure of optimization of each subsystem-based MPC in this method, the states of other subsystems are approximated to the prediction of previous instant. To enhance the efficiency of DMPC solution, Li et al. developed an iterative algorithm for DMPC based on Nash optimality for large-scale LTI processes in [22]. The whole system will arrive at Nash equilibrium if the convergent condition of the algorithm is satisfied. Also, in [23], a DMPC method with guaranteed feasibility properties is presented. This method allows the practitioner to terminate the distributed MPC algorithm at the end of the sampling interval, even if convergence is not attained. However, as pointed out by the authors of [22–25], the performance of the DMPC framework is, in most cases, different from that of centralized MPC. In order to guarantee performance improvement and the appropriate communication burden among subsystems, an extended scheme based on a so called "neighbourhood optimization" is proposed in [24], in which the optimization objective of each subsystem-based MPC considers not only the performance of the local subsystem, but also those of its neighbours. The HSLC process is a nonlinear, large-scale system and each subsystem is coupled with its neighbours by states, so it is necessary to design a new DMPC framework to optimize HSLC process. This DMPC framework should be suitable for nonlinear system with fast computational speed, appropriate communication burden and good global performance.

In this work, each local MPC of the DMPC framework proposed is formulated based on successive on-line linearization of nonlinear model to overcome the computational obstacle caused by nonlinear model. The prediction model of each MPC is linearized around the current operating point at each time instant. Neighbourhood optimization is adopted in each local MPC to improve the global performance of HSLC and lessen the communication burden. Furthermore, since the strip temperature can only be measured at a few positions due to the hard ambient conditions, EKF is employed to estimate the transient temperature of strip in the water cooling section.

The contents are organized as follows. Section 2 describes the HSLC process and the control problem. Section 3 presents proposed control strategy of HSLC, which includes the modelling of subsystems, the designing of EKF, the functions of predictor and the development of local MPCs based on neighbourhood optimization for subsystems, as well as the iterative algorithm for solving the proposed DMPC. Both simulation and experiment results are presented in Section 4. Finally, a brief conclusion is drawn to summarize the study and potential expansions are explained.

2. Laminar cooling of hot-rolled strip

2.1. Description

The HSLC process is illustrated in Fig. 1. Strips enter cooling section at finishing rolling temperature (FT) of 820–920 °C, and are coiled by coiler at coiling temperature (CT) of 400–680 °C after being cooled in the water cooling section. The X-ray gauge is used to measure the gauge of strip. Speed tachometers for measuring coiling speed is mounted on the motors of the rollers and the mandrel of the coiler. Two pyrometers are located at the exit of finishing mill and before the pinch rol1 respectively. Strips are 6.30–13.20 mm in thickness and 200–1100 m in length. The run-out table has 90 top headers and 90 bottom headers. The top headers are of U-type for laminar cooling and the bottom headers are of straight type for low pressure spray. These headers are divided into 12 groups. The first nine groups are for the main cooling section and the 1ast three groups are for the fine cooling section. In this HSLC, the number of cooling water header groups and the water flux of each header group are taken as control variables to adjust the temperature distribution of the strip.

2.2. Thermodynamic model

Consider the whole HSLC process from the point of view of geometrically distributed setting system (The limits of which are represented by the geometrical locations of FT and CT, as well as the strip top and bottom sides), a two dimensional mathematical model for Cartesian coordinates is developed combining academic and industrial research findings [26]. The model assumes that there is no direction dependency for the heat conductivity λ. There is no heat transfer in traverse and rolling direction. The latent heat is considered by using temperature-dependent thermal property developed in [27] and the model is expressed as

$$\dot{x} = \frac{-\lambda}{\rho c_p}\frac{\partial^2 x}{\partial z^2} - \dot{l}\cdot\frac{\partial x}{\partial l} \tag{1}$$

with the boundary conditions on its top and bottom surfaces

$$\pm\lambda\frac{\partial x}{\partial z} = h\cdot(x - x_\infty) \tag{2}$$

where the right hand side of (2) is h times $(x - x_\infty)$ and

$$h = h_w\frac{x - x_w}{x - x_\infty} + \sigma_0\varepsilon\frac{x^4 - x_\infty^4}{x - x_\infty} \tag{3}$$

and $x(z, l, t)$ strip temperature at position (z, l);

l, z length coordinate and thickness coordinate respectively;
ρ density of strip steel;
c_p specific heat capacity;
λ heat conductivity;
σ_0 Stefan–Boltzmann constant (5.67×10^{-8} w/m^2 K^4);

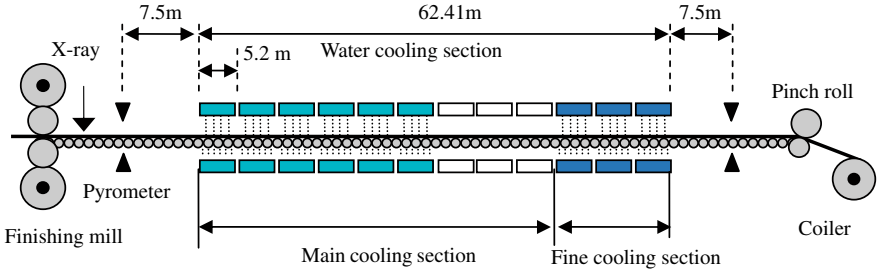

Fig. 1. Hot-rolled strip laminar cooling process.

ε emission coefficient $((x/1000)\cdot[0.125x/1000-0.38]+1.1)$;
x_∞ ambient temperature;
h_w convection heat transfer coefficient (W/mm^2 °C) on the surface of strip.

The radiation boundary condition is only applicable out of the water cooling section. The transfer coefficient h_w is only applicable in the water cooling section and is calculated as follows:

$$h_w = \alpha\frac{2186.7}{10^6}\left(\frac{x}{x_0}\right)^a\left(\frac{v}{v_0}\right)^b\left(\frac{F}{F_0}\right)^c \tag{4}$$

where $x_0 = 1000$ °C, $v_0 = 20$ m/s, $F_0 = 350$ m^3/(m^2 min), $a = 1.62$, $b = -0.4$, $c = 1.41$, v is the velocity of strip and F is the flux of cooling water.

2.3. Problem statement

The technical targets of HSLC refer to CT and the temperature drop curve of strip caused by cooling water. Contemplating the overall system from the point of view of the geometrically distributed setting system, as shown in Fig. 2, we can transform the desired temperature drop curve of strip into the geometrically location-dependent temperature profile from finishing mill to coiler. Here the temperature on desired cooling curve refers to strip's average temperature in thickness direction. Therefore, the control objective becomes to adjust the average temperature of strip in thickness direction to be consistent with the geometrically location-dependent temperature profile. The manipulated variables of system are the states (opening or closing) and the water fluxes of every header groups.

2.3.1. Existing method

The existing method in industrial manufactory is open-loop and closed-loop method. The open-loop part charges the main cooling section and the closed-loop part charges the fine cooling section. The water fluxes of all opening headers in main cooling section are constant and are the same to each others, which are determined by expert experience according to the cooling rate in the first section of cooling curve. The number of header groups opened in the main cooling section N_{ho} is used to adjust the strip temperature at the exit of main cooling section, and is calculated online according to the feed-forward signal of FT at each control period as follows:

$$N_{ho} = \mathrm{int}\left(\frac{x_{FT}-x_{cm}}{CR_m}\right)$$

where x_{cm} is the reference temperature at the exit of main cooling section; x_{FT} is the finishing rolling temperature; CR_m is the reference cooling rate in main cooling section. In the closed-loop part, a PI controller is employed to control the water flux in fine cooling section according to the feed-back measurement of CT.

However, in this method, some inaccurate or unreasonable assumptions are applied additionally for the simplification of this large-scale system (e.g. the cooling rate in main cooling section is impossible to be constant if the water flux of every headers keeps to be the same value), which makes the system less flexibility for various cooling curves and be less precise. On the other hand, since the major disturbance (the fluctuation of x_{cm}) does not feed into PI controller in closed-loop part, it is also difficult to achieve an accurate CT. Thus this control method is hard to satisfy the increasing quality requirements of steel industry.

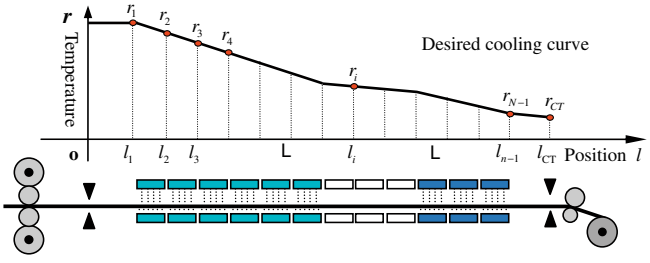

Fig. 2. Desired temperature profile.

2.3.2. Why using DMPC framework

To obtain productions with better quality, a suitable optimization method is required for making the average temperature of strip in thickness direction consistent with the desired temperature profile at any position of the water cooling section. To realize it, we should consider the water flux of each header group as an individual manipulated variable rather than consider all of them as one or two manipulated variables simply. That means the control method should be suitable for large-scale, nonlinear and relatively fast MIMO system. Furthermore, this optimization method should be able to account for the major measurable disturbance of FT online for precision enhancing.

MPC is widely recognized as practical and well performed control technology [7] for process control, especially for MIMO system. The measurable disturbance can also be taken into account through the prediction model of MPC. Thus, MPC can be a good selection for this system. As is shown in Fig. 2, the desired geometrically location-dependent temperatures are selected at the locations $l_1, l_2, \ldots, l_N$ as the reference temperatures with the notation

$$\boldsymbol{r} = [r_1\ r_2 \cdots r_N]^{\mathrm{T}} \tag{5}$$

Here, $l_1, l_2, \ldots, l_N$ correspond to the locations of the exit of each header group and the locations of the pyrometers used to measure FT and CT. The optimization objective is to minimize

$$J = \sum_{t=1}^{P}\|\boldsymbol{y}(k+t|k)-\boldsymbol{r}(k+t)\|_{\boldsymbol{Q}}^2 + \sum_{h=1}^{M}\|\Delta\boldsymbol{u}(k+h-1|k)\|_{\boldsymbol{R}}^2 \tag{6}$$

where $\boldsymbol{y} = [y_1, \ldots, y_N]^{\mathrm{T}}, y_s (s = 1, \ldots, N)$ is the average temperature of strip at position l_s; $\mathbf{u}$:the manipulated variable vector, refers to the future sequence of water flux; $\Delta\boldsymbol{u}$ is the increment of manipulated variable vector $\boldsymbol{u}$; P is the prediction horizon and M is the control horizon. The weighting matrices $\boldsymbol{Q}$ and $\boldsymbol{R}$ are positive definite and have block-diagonal forms.

However, for this large-scale, nonlinear and relatively fast system, the on-line implementation of centralized MPC is impractical due to the large computation. To decrease the computational burden and guarantee the performance of overall system at the same time, a DMPC framework based on neighbourhood optimization and successive linearization is therefore proposed for HSLC.

3. Control strategy of HSLC

Since the major obstacle of accurate online control of HSLC is the large-scale, nonlinear characteristics, the DPMC framework is adopted. The whole system is divided into N subsystems (The sth subsystem ranges from l_{s-1} to l_s $(s = 1, 2, \ldots, N)$ as shown in Fig. 2.), and each subsystem is controlled by a local MPC controller as shown in Fig. 3. Since the strip temperature can only be measured at a few positions inside the cooling section due to the hard ambient conditions, an EKF is employed to estimate the distribution of strip temperature. Each local MPC calculates the set-point of PI controller based on the current strip temperature estimated by EKF and the future states of its neighbours. Each PI controller regulates water flux to be consistent with the set-point calculated by local MPC. Since there are no manipulated variables in the subsystems with closed header group, a predictor is substituted

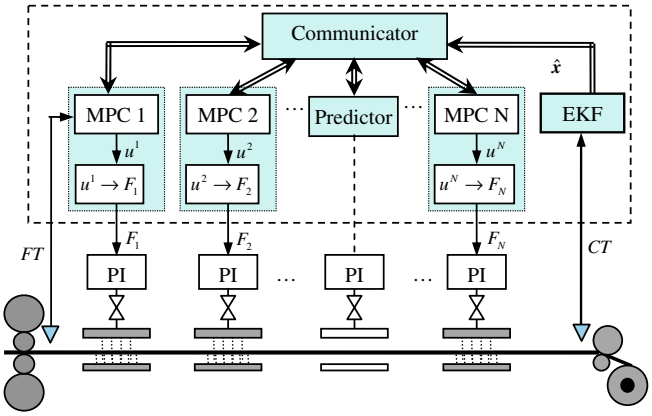

Fig. 3. The structure of DMPC framework for HSLC.

for local MPC. The predictor estimates the future states of corresponding subsystem and broadcasts the estimations to its neighbours. In this way, the EKF, MPCs and predictors, as well as the PI controllers work together through network information to control the HSLC.

3.1. State space model of subsystems

Since it is not easy for MPC to predict the future states using model Eq. (1), the state space representation of model Eq. (1) for each subsystem is deduced first in this subsection. Using 2D finite volumes scheme [28], model Eq. (1) can be reduced into a finite dimensional problem. In each subsystem s, denote the number of volumes in l-direction by n_s and z-direction by m as shown in Fig. 4. Each volume, denoted by V, equals to $\Delta l \Delta z$.. Δl and Δz are the length and thickness of each volume respectively. Denote the temperature of the ith z-direction and the jth l-direction volume by $x^s_{i,j}$.

Let

$$x^0_{i,n_s} = x_{FT}, \quad i = 1,2,\ldots,m. \tag{7}$$

$$x^N_{i,n_s} = x^N_{i,n_s-1}, \quad i = 1,2,\ldots,m. \tag{8}$$

The energy balance Eq. (1) being applied to the top surface and bottom surface volumes leads to

$$\dot{x}^s_{1,j} = -\frac{\lambda^s_{1,j}}{\rho^s_{1,j} cp^s_{1,j}}\left(\frac{1}{\Delta z^2}\left(x^s_{2,j} - x^s_{1,j} - \Delta z \frac{h^s_{1,j}}{\lambda^s_{1,j}}(x^s_{1,j} - x_\infty)\right)\right) - \frac{1}{\Delta l}\cdot v(x^s_{1,j} - x^s_{1,j-1}) \tag{9}$$

$$\dot{x}^s_{m,j} = -\frac{\lambda^s_{m,j}}{\rho^s_{m,j} cp^s_{m,j}}\left(\frac{1}{\Delta z^2}\left(x^s_{m-1,j} - x^s_{m,j} - \Delta z \frac{h^s_{m,j}}{\lambda^s_{m,j}}(x^s_{m,j} - x_\infty)\right)\right) - \frac{1}{\Delta l}\cdot v(x^s_{m,j} - x^s_{m,j-1}) \tag{10}$$

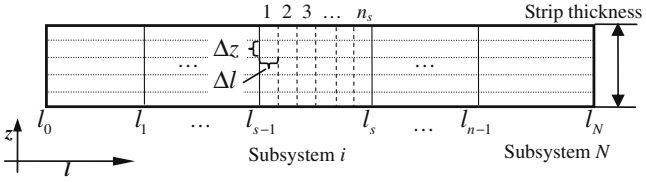

Fig. 4. The division of each subsystem.

For the internal volumes, it comes

$$\dot{x}^s_{i,j} = -\frac{1}{\Delta z^2}\frac{\lambda^s_{i,j}}{\rho^s_{i,j} cp^s_{i,j}}(x^s_{i+1,j} - 2x^s_{i,j} + x^s_{i-1,j}) - \frac{1}{\Delta l}\cdot v(x^s_{i,j} - x^s_{i,j-1}) \tag{11}$$

where $v = \dot{l}$ is the coiling velocity; $x^s_{i,j-1} = x^{s-1}_{i,n_{s-1}}$ when $j = 1$ and $x^s_{i,j+1} = x^{s+1}_{i,1}$ when $j = n_s$.

In industrial application, the measurements are available digitally with a sampling time Δt. Thus the discrete-time version of the subsystem is derived by approximating the derivatives using simple Euler approximation. Since $\rho^s_{i,j}$, $\lambda^s_{i,j}$ and $cp^s_{i,j}$ are temperature dependent, define $a(x^s_{i,j}) = -\Delta t \lambda^s_{i,j}/(\Delta z^2 \rho^s_{i,j} cp^s_{i,j})$, $\beta(x^s_{i,j}) = \Delta t \cdot a^s_{i,j}/\lambda^s_{i,j}$ and $\gamma = \Delta t \cdot v/\Delta l$. Then the nonlinear state space representation of subsystem s deduced from the previous Eqs. (7)–(11) can be expressed as

$$\begin{cases} \boldsymbol{x}^s(k+1) = \boldsymbol{f}(\boldsymbol{x}^s(k))\cdot \boldsymbol{x}^s(k) + \boldsymbol{g}(\boldsymbol{x}^s(k))\cdot u^s(k) + \boldsymbol{D}\cdot \boldsymbol{x}^{s-1}_{n_{s-1}}(k) \quad s = 1,2,\ldots,N \\ y^s(k) = \boldsymbol{C}\cdot \boldsymbol{x}^s(k) \end{cases} \tag{12}$$

where

$$\begin{aligned} &\boldsymbol{x}^s = [(\boldsymbol{x}^s_1)^{\mathrm{T}}\ (\boldsymbol{x}^s_2)^{\mathrm{T}}\ \cdots\ (\boldsymbol{x}^s_{n_s})^{\mathrm{T}}]^{\mathrm{T}}; \\ &\boldsymbol{x}^s_j = [x^s_{1,j}\ x^s_{2,j}\cdots\ x^s_{m,j}]^T, \quad (j = 1,2,\ldots,n_s); \end{aligned} \tag{13}$$

is the state vector of subsystem s, y^s is the average temperature of the last column volumes of subsystem s, u^s is the input of subsystem s and is defined as follows:

$$\begin{cases} u^s = 2186.7\times 10^{-6}\times \alpha\cdot(v/v_0)^b\times(F_s/F_0)^c, & s\in \boldsymbol{C_W} \\ u^s = 1, & s\in \boldsymbol{C_A} \end{cases} \tag{14}$$

where $\mathscr{C}_{\mathscr{W}}$ is the set of subsystems in which strips are cooled by water, and $\mathscr{C}_{\mathscr{A}}$ is the set of subsystems in which strips are cooled major through radiation. $\boldsymbol{f}(\boldsymbol{x}^s(k))$, $\boldsymbol{g}(\boldsymbol{x}^s(k))$, $\boldsymbol{D}$ and $\boldsymbol{C}$ are coefficient matrices of subsystem s, and are defined as follows:

$$\boldsymbol{f}(\boldsymbol{x}^s(k)) = \begin{bmatrix} \boldsymbol{\Phi}_1(\boldsymbol{x}^s(k))\cdot\boldsymbol{\Lambda} & \boldsymbol{0} & \cdots & \boldsymbol{0} \\ \boldsymbol{0} & \boldsymbol{\Phi}_2(\boldsymbol{x}^s(k))\cdot\boldsymbol{\Lambda} & & \vdots \\ \vdots & & \ddots & \boldsymbol{0} \\ \boldsymbol{0} & \cdots & \boldsymbol{0} & \boldsymbol{\Phi}_{n_s}(\boldsymbol{x}^s(k))\cdot\boldsymbol{\Lambda} \end{bmatrix} + \begin{bmatrix} (1-\gamma)\boldsymbol{I}_m & \boldsymbol{0} & \cdots & \boldsymbol{0} \\ \gamma\boldsymbol{I}_m & (1-\gamma)\boldsymbol{I}_m & \ddots & \vdots \\ \vdots & \ddots & \ddots & \boldsymbol{0} \\ \boldsymbol{0} & \cdots & \gamma\boldsymbol{I}_m & (1-\gamma)\boldsymbol{I}_m \end{bmatrix} \tag{15}$$

$$\boldsymbol{g}(\boldsymbol{x}^s(k)) = \left[\boldsymbol{\psi}_1(\boldsymbol{x}^s(k))^{\mathrm{T}}\cdots\boldsymbol{\psi}_{n_s}(\boldsymbol{x}^s(k))^{\mathrm{T}}\right]^{\mathrm{T}}; \tag{16}$$

$$\boldsymbol{C} = m^{-1}\cdot[\boldsymbol{0}^{1\times m\cdot(n_s-1)}\boldsymbol{1}^{1\times m}]; \tag{17}$$

$$\boldsymbol{D} = [\gamma\boldsymbol{I}_m\ \boldsymbol{0}^{m\times m\cdot(n_s-1)}]^{\mathrm{T}}; \tag{18}$$

and

$$\boldsymbol{\Phi}_j(\boldsymbol{x}^s) = \begin{bmatrix} a(x^s_{1,j}) & \cdots & 0 \\ \vdots & \ddots & \vdots \\ 0 & \cdots & a(x^s_{m,j}) \end{bmatrix};$$

$$\boldsymbol{\psi}_j(\boldsymbol{x}^s) = \begin{bmatrix} \theta^s_{1,j}(x^s_{1,j})(x^s_{1,j} - x_\infty)\cdot\beta(x^s_{1,j}) \\ \boldsymbol{0}^{(m-2)\times 1} \\ \theta^s_{m,j}(x^s_{m,j})(x^s_{m,j} - x_\infty)\cdot\beta(x^s_{m,j}) \end{bmatrix};$$

$$\boldsymbol{\Lambda} = \begin{bmatrix} -1 & 1 & 0 & \cdots & 0 \\ 1 & -2 & 1 & \ddots & \vdots \\ 0 & \ddots & \ddots & \ddots & 0 \\ \vdots & \ddots & 1 & -2 & 1 \\ 0 & \cdots & 0 & 1 & -1 \end{bmatrix}; \quad \boldsymbol{I}_m \in R^{m\times m}; \quad (j = 1,2,\ldots,n_s);$$

$$\begin{cases} \theta^s_{i,j}(x^s_{i,j}) = (x^s_{i,j}/x_0)^a, & s \in \mathscr{C}_{\mathscr{W}}, \quad (i = 1,2,\ldots,m, j = 1,2,\ldots,n_s) \\ \theta^s_{i,j}(x^s_{i,j}) = h_{air}(x^s_{i,j}), & s \in \mathscr{C}_{\mathscr{A}} \end{cases} \tag{19}$$

It should be noticed that the notations $\boldsymbol{g}^s(\cdot)$ and u^s are different between the subsystems which belong to $\mathscr{C}_{\mathscr{A}}$ and the subsystems which belong to $\mathscr{C}_{\mathscr{W}}$, see (14) and (19). Since the current states of subsystems are not measurable inside the cooling section, an observer is designed to estimate the current states of each subsystem in the next subsection.

3.2. Design of Extended Kalman Filter

The nonlinear model of the overall system can be expressed as

$$\begin{cases} \boldsymbol{x}(k+1) = \boldsymbol{F}(\boldsymbol{x}(k))\boldsymbol{x}(k) + \boldsymbol{G}(\boldsymbol{x}(k))\boldsymbol{u}(k) + \bar{\boldsymbol{D}}\boldsymbol{x}^0(k) \\ \bar{\boldsymbol{y}}(k) = \bar{\boldsymbol{C}}\boldsymbol{x}(k) \end{cases} \tag{20}$$

where $\boldsymbol{x} = [(\boldsymbol{x}^1)^{\mathrm{T}}(\boldsymbol{x}^2)^{\mathrm{T}}\ldots(\boldsymbol{x}^N)^{\mathrm{T}}]^{\mathrm{T}}$ and $\boldsymbol{u} = [u^1u^2\ldots u^{n_s}]^{\mathrm{T}}$, $\boldsymbol{x}^0$ is the distribution of FT in z-direction. $\bar{\boldsymbol{y}}$ is the output vector which includes the measurements of CT on the top and bottom surfaces. The expressions of $\boldsymbol{F}(\boldsymbol{x}(k)), \boldsymbol{G}(\boldsymbol{x}(k))$ and $\bar{\boldsymbol{D}}$ can be deduced easily from (12). Coefficient matrix $\bar{\boldsymbol{C}}$ is defined as

$$\bar{\boldsymbol{C}} = \begin{bmatrix} \boldsymbol{0}^{1\times(N-1)n_sm} & 1 & \boldsymbol{0}^{1\times(n_sm-1)} \\ \boldsymbol{0}^{1\times(N-1)n_sm} & \boldsymbol{0}^{1\times(n_sm-1)} & 1 \end{bmatrix} \tag{21}$$

This system is uniformly observable because each volume's temperature depends on its neighbours. Since the order of system is inevitably high, the famous EKF is chosen to be more convenient to design in our case. The estimating of the strip temperature distribution can be expressed as

$$\hat{\boldsymbol{x}}(k+1) = \hat{\boldsymbol{x}}(k+1|k) + \boldsymbol{K}_{k+1}(\bar{\boldsymbol{y}}(k+1) - \bar{\boldsymbol{C}}\hat{\boldsymbol{x}}(k+1|k)) \tag{22}$$

The feedback coefficient $\boldsymbol{K}_{k+1}$ is deduced by *difference Riccati equation* [29]. This observer estimates the states of overall system at each control period, and transmits them to all subsystems.

3.3. Predictor

Since there are no manipulated variables in subsystem $s \in \mathscr{C}_{\mathscr{A}}$, a predictor is applied for estimating the future states $\boldsymbol{X}_s(k)$ where

$$\boldsymbol{X}_s(k) = [\boldsymbol{x}^s(k+1)\boldsymbol{x}^s(k+2)\cdots\boldsymbol{x}^s(k+P)]^{\mathrm{T}} \tag{23}$$

In the predictor, the prediction model is (12), and the measurable disturbance FT is assumed to be a constant during the estimating of $\boldsymbol{X}_1(k)$.

When finishing estimating $\boldsymbol{X}_s(k)$, the predictor sends the estimation of $\boldsymbol{X}_s(k)$ to the downstream neighbours of subsystem s.

3.4. Local MPC formulation

As for subsystem $s \in \mathscr{C}_{\mathscr{W}}$, the strip temperature is controlled by a local MPC. The local MPC is formulated based on neighbourhood optimization and successive linearization of prediction model. The details of it are presented as follows.

Since the weighting matrices $\boldsymbol{Q}$ and $\boldsymbol{R}$ have block-diagonal forms in (6), the global performance index can be decomposed in terms of the local indices for each subsystem [30]

$$\begin{aligned} J_s(k) = &\sum_{i=1}^{P} \|\boldsymbol{r}_s(k+i) - \hat{\boldsymbol{y}}^s(k+i|k)\|^2_{\boldsymbol{Q}_s} \\ &+ \sum_{h=1}^{M} \|\Delta u^s(k+h-1|k)\|^2_{R_s}, \quad (s = 1,2,\ldots,N) \end{aligned} \tag{24}$$

The local control decision is computed by solving local optimization problem $J_s(k)$ with local input/output variables and constraints. However, the optimal solution to the local optimization problem collectively is not equal to the global optimal control decision of the whole system. To enhance the global control performance, neighbourhood optimization is adopted.

Define the set of the subsystems whose states are affected by the states of subsystem s as downstream neighbourhood of subsystem s, and denote it by π_{-s}, $s \notin \pi_{-s}$.

Similarly, define the set of subsystems whose states affect the states of subsystem s as upstream neighbourhood of subsystem s, and denote it by π_{+s}, $s \notin \pi_{+s}$.

Since the future states of the downstream neighbours are affected by the future inputs of subsystem s, the new performance index for each subsystem can be improved by

$$\min \bar{J}_s(k) = \sum_{j\in\{\pi_{-s},s\}} J_j(k) \tag{25}$$

Notice that the new performance index for the sth subsystem $\bar{J}_s(k)$ is composed not only of cost function of subsystem s but also of its downstream neighbours', which is called by *neighbourhood optimization* [24]. Cooperation between subsystems is achieved by exchanging information between each subsystem and its neighbours in a distributed structure via network communication and by optimizing the local problem with the new performance index (25).

It should be noticed that model Eq. (12) is a nonlinear model. If the future evolution of each subsystem is predicted through it, the minimization of a quadratic index, subject to the nonlinear HSLC dynamic, would be a nonlinear optimization problem. This can be computationally demanding, depending on the states and constraints. To overcome this problem, the prediction model is linearized around the current operating point at each time step, and a linear MPC is designed for the resulting linear system. The idea of using time varying models traces back to the early 1970s in the process control field although it has been properly formalized only recently. Studies on linear parameter varying MPC schemes can be found in [31–33,13,34]. Among them, the works in [33,13] and [34] are the closest to our approach.

In this case, the following prediction model is used to approximate the nonlinear model Eq. (12) at time instant k

$$\begin{cases} \boldsymbol{x}^s(i+1|k) = \boldsymbol{A}_s(k)\cdot\boldsymbol{x}^s(i|k) + \boldsymbol{B}_s(k)\cdot u_s(i|k) + \boldsymbol{D}\cdot\boldsymbol{x}^{s-1}_{n_{s-1}}(i|k) \\ y^s(i|k) = \boldsymbol{C}\cdot\boldsymbol{x}^s(i|k) \end{cases} s = 1,2,\ldots,N \tag{26}$$

where $\boldsymbol{A}_s(k) = \boldsymbol{f}(\boldsymbol{x}^s(k))$ and $\boldsymbol{B}_s(k) = \boldsymbol{g}(x^s(k))$. The $(s-1)$th subsystem and the $(s+1)$th subsystem are the upstream neighbour and the downstream neighbour of subsystem s respectively. Assuming that $\boldsymbol{x}(k)$ is available, the local optimization problem for subsystem s at the sampling time instant k becomes

$$\begin{aligned} \min_{\Delta U_s(k)} \quad & \bar{J}_s(k) = \sum_{j\in\{s,s+1\}} \left(\sum_{i=1}^{P} \|\boldsymbol{r}_j(k+i) - \hat{\boldsymbol{y}}^j(k+i|k)\|^2_{\boldsymbol{Q}_j} \right. \\ & \left. + \sum_{h=1}^{M} \|\Delta u^j(k+h-1|k)\|^2_{R_j} \right) \\ s.t. \quad & \boldsymbol{x}^j(i+1|k) = \boldsymbol{A}_j(k)\cdot\boldsymbol{x}^j(i|k) + \boldsymbol{B}_j(k)\cdot u^j(i|k) + \boldsymbol{D}\cdot\boldsymbol{x}^{j-1}_{n_{j-1}}(i|k), \\ & j \in \{s,s+1\} \\ & \boldsymbol{u}^s_{\min} \leqslant \boldsymbol{u}^s(k+h-1|k) \leqslant \boldsymbol{u}^s_{\max}, \quad h = 1,\cdots,M \\ & \Delta\boldsymbol{u}^s_{\min} \leqslant \Delta\boldsymbol{u}^s(k+h-1|k) \leqslant \Delta\boldsymbol{u}^s_{\min}, \quad h = 1,\cdots,M \\ & \boldsymbol{x}^j_{\min} \leqslant \boldsymbol{x}^j(k+i|k) \leqslant \boldsymbol{x}^j_{\min}, \quad i = 1,\cdots,P,\ j \in \{s,s+1\} \end{aligned} \tag{27}$$

where $\{\boldsymbol{u}^s_{\min}, \boldsymbol{u}^s_{\max}\}, \{\Delta\boldsymbol{u}^s_{\min}, \Delta\boldsymbol{u}^s_{\max}\}$ and $\{\boldsymbol{x}^j_{\min}, \boldsymbol{x}^j_{\max}\}(j \in \{s,s+1\})$ are boundaries of manipulated variables, increment of manipulated variables and state vectors respectively, and

$$\Delta \boldsymbol{U}_s(k) = [\Delta u^s(k)\Delta u^s(k+1)\cdots\Delta u^s(k+M)]^{\mathrm{T}} \tag{28}$$

Define that

$$\begin{aligned}\boldsymbol{X}_{s,n_s}(k) &= [\boldsymbol{x}^s_{n_s}(k+1)\boldsymbol{x}^s_{n_s}(k+2)\cdots\boldsymbol{x}^s_{n_s}(k+P)]^{\mathrm{T}}\\ \boldsymbol{U}_s(k) &= [u^s(k)u^s(k+1)\cdots u^s(k+M)]^{\mathrm{T}}\end{aligned} \tag{29}$$

If sequences $\boldsymbol{X}_{s-1,n_{s-1}}(k)$ and $\boldsymbol{U}_{s+1}(k)$ are available to subsystem s, problem (27) can be recast as a quadratic program (QP). Then optimal control decision sequence $\Delta\boldsymbol{U}^*_s(k)$ of subsystem s can be computed at time instant k by solving (27) for the current states. The first sample of $\boldsymbol{U}^*_s(k) = u^s(k-1)\boldsymbol{I}_{1\times M} + \Delta\boldsymbol{U}^*_s(k)$, is used to compute the optimal water flux set-point of subsystem s according to (14).

We remark that model Eq. (12) is linearized around an operating point that, in general, it is not an equilibrium point. When evaluating the on-line computational burden of the proposed scheme, one needs to account for the resources spent in computing the linear model Eq. (26) and translating (27) into a standard quadratic programming (QP) problem. Nevertheless, for the proposed application, complexity of problem (27) is reduced greatly comparing to the nonlinear model based MPC.

3.5. Iterative algorithm

According to the neighbourhood optimization, the local optimal control decision for each subsystem can be obtained by solving problem (27) if the local optimal control decision of its downstream neighbours and the future optimal states of its upstream neighbours are available, that is

$$\Delta\boldsymbol{U}^*_s(k) = \arg\left\{\min_{\Delta U_s(k)} \bar{J}_s(k)|_{U^*_j(k)(j\in\mathscr{N}_{-i}, j\neq i), \boldsymbol{X}^*_h(k)(h\in\mathscr{N}_{+i}, h\neq i)}\right\} \quad (s=1,\cdots,N) \tag{30}$$

However, the local optimal control decision of its downstream neighbours and the future optimal states of its upstream neighbours are not available to subsystem s, and hence the estimations of them are used. To get an accurate solution of problem (27), an iterative algorithm is developed to seek the local optimal control decision for each subsystem at each sampling period.

Distributed MPC algorithm:

Step 1. *Initialization and communication:* At the sampling instant k, the EKF sends the current states of the system to the corresponding subsystem. Each subsystem initializes the estimation of local optimal control decision and transmits it to its upstream neighbours. Set the iterative index $l = 0$:

$$\boldsymbol{U}^{(l)}_s(k) = \hat{\boldsymbol{U}}_s(k), \quad (s=1,2,\ldots,N)$$

Each subsystem calculates the estimate of local state sequence $\boldsymbol{X}^{(l)}_s(k)$ by (26) and transmits them to its downstream neighbours through network.

Step 2. *Subsystem optimization:* Each subsystem which belongs to $\mathscr{C}_{\mathscr{W}}$ solves its local optimization problem described in (27) simultaneously to derive its control decision. That is

$$\Delta\boldsymbol{U}^{(l+1)}_s(k) = \arg\left\{\min_{\Delta U_s(k)} \bar{J}_s(k)|_{U^{(l)}_j(k)(j\in\mathscr{N}_{-i}), \boldsymbol{X}^{(l)}_h(k)(h\in\mathscr{N}_{+i})}\right\}$$

$$\boldsymbol{U}^{(l+1)}_s(k) = u^s(k-1)\boldsymbol{I}_{1\times M} + \Delta\boldsymbol{U}^{(l+1)}_s(k), \quad s\in\mathscr{C}_{\mathscr{W}}$$

Set the optimal solution of each subsystem belonging to $\mathscr{C}_{\mathscr{A}}$

$$\boldsymbol{U}^{(l+1)}_s(k) = [11\cdots1]^{\mathrm{T}}, \quad s\in\mathscr{C}_{\mathscr{A}}.$$

Then, calculate the estimation of local state sequence $\boldsymbol{X}^{(l)}_s(k)$ by (26).

Step 3. *Checking and updating:* Each subsystem checks if its terminal iteration condition is satisfied, that is, for the given error tolerance $\varepsilon_s \in \mathbb{R}(s=1,\ldots,N)$, if there exists

$$\|\boldsymbol{U}^{(l+1)}_s(k) - \boldsymbol{U}^{(l)}_s(k)\| \leqslant \varepsilon_s \quad (s=1,\cdots,N).$$

If all the terminal conditions are satisfied at iteration l^*, then stop the iteration, set the local optimal control decision for each subsystem $\boldsymbol{U}^*_s(k) = \boldsymbol{U}^{(l^*)}_s(k)$, and go to **Step 4**; otherwise, let $l = l+1$, each subsystem transmits the new information $\boldsymbol{U}^{(l)}_s(k)$ to its upstream neighbours and transmits $\boldsymbol{X}^{(l)}_s(k)$ to its downstream neighbours, and go to **Step 2**;

Step 4. *Assignment and implementation*: Each subsystem computes the control law

$$u^{s^*}(k) = [10\cdots0]\boldsymbol{U}^*_s(k). \quad (s=1,\cdots,N)$$

and apply it to the corresponding subsystem.

Step 5. *Reassigning the initial estimation*: Set the initial estimate of the local optimal control decision for the next sampling time

$$\hat{\boldsymbol{U}}_s(k+1) = \boldsymbol{U}^*_s(k) \quad (s=1,\ldots,N);$$

Step 6. *Receding horizon:* Move horizon to the next sampling time, that is $k+1\to k$, go to **Step 1**, and repeat the above steps.

The on-line optimization of HSLC, which is a large-scale nonlinear system, is converted into several small-scale systems via distributed computation, thus computational complexity is significantly reduced. In addition, information exchange among neighbouring subsystems in a distributed structure via communication can improve control performance. Through this method, the whole temperature evolution of the strip is controlled online, which provides possibilities of producing many new types of steel with high quality (e.g. the multi-phase steel). To prove the validation of the proposed strategy, both numerical simulations and experiments on a HSLC experimental apparatus are implemented in the next section.

4. Numerical experiment

To test the validation of the proposed method, low carbon C2 type steel is taken as an example. The parameters of C2 strip steel are shown in Table 1.

Table 1
Thermal and physical properties of the strip.

Item	Value	Units
Thermal conductivity $\lambda^s_{i,j}$	$\begin{cases}56.43-(0.0363-c(v-v_0))\times x^s_{0,j}\\ 56.43-(0.0363-c(v-v_0))\times x^s_{m,i}\end{cases}$	$\mathrm{W\,m^{-1}\,K^{-1}}$
Thermal diffusivity $a(x^s_{i,j})$	$\begin{cases}8.65+(5.0-8.65)(x^s_{i,j}-400)/250 & x^s_{i,j}\in[400,650)\\ 5.0+(2.75-5.0)(x^s_{i,j}-650)/50 & x^s_{i,j}\in[650,700)\\ 2.75+(5.25-2.75)(x^s_{i,j}-700)/100 & x^s_{i,j}\in[700,800)\\ 5.25+0.00225(x^s_{i,j}-800) & x^s_{i,j}\in[800,1000]\end{cases}$	$\times10^{-6}\,\mathrm{m^2\,s^{-1}}$
Temperature of ambient	25 + 273.5	K
Temperature of cooling water	25 + 273.5	K

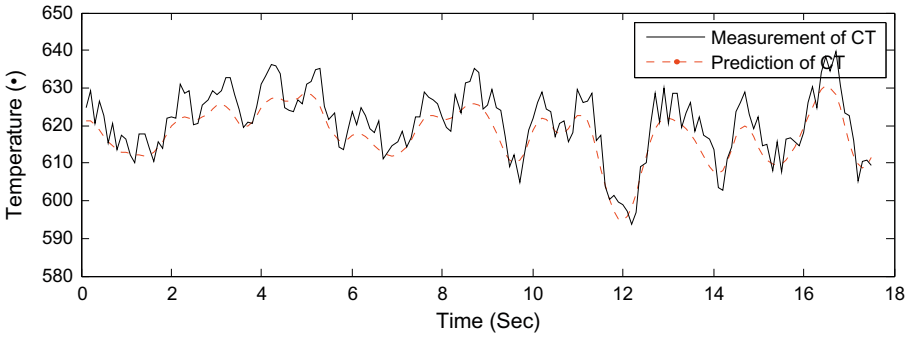

Fig. 5. Comparison between the predictive CT and the measurement of CT.

4.1. Validation of designed model

An experiment on full scale industrial plant is performed with a strip of 3.51 mm in thickness to test the validation of the designed model. In the experiment, the spatial meshing chosen to validate the model is composed of 5 volumes of 0.7 mm in thickness and 30 volumes of 2.7 m in length, that is $m = 5$, $n = 30$. The water fluxes in the main cooling section and in the fine cooling section equal to 150 $m^3/(s\ m^2)$ and 75 $m^3/(m^2\ s)$ respectively. The resulting prediction of CT and the measurement of CT are shown in Fig. 5. The curve of predictive CT is very close to that of measurement. The phenomenon that the predictive curve is smoother than the measurement curve is caused by the second term in the right hand side of model Eq. (1).

4.2. Convergence of EKF

The convergence of EKF is verified through a simulation here. The initial states (the temperature of each volume) of process model and observer are shown in Fig. 6, where the initial states of the observer are 30 °C higher than those of the process model. The states of header groups are [1, 1, 1, 1, 1, 1, 0, 0, 0, 1, 1, 1], where one stands for opening and zero means closing. The coiling speed v equals to 10.74 m s^{-1}. The water fluxes in the main cooling section and the fine cooling section are 200 $m^3/(s\ m^2)$ and 150 $m^3/(s\ m^2)$ respectively. FT is 870 °C. For spatial reason, the temperatures of 2nd, 6th, 10th and 14th subsystems at layers from top surface to central of strip are selected as examples to illustrate the convergence of EKF. Fig. 7 shows that the temperatures observed by EKF are convergent to temperatures estimated by the process model.

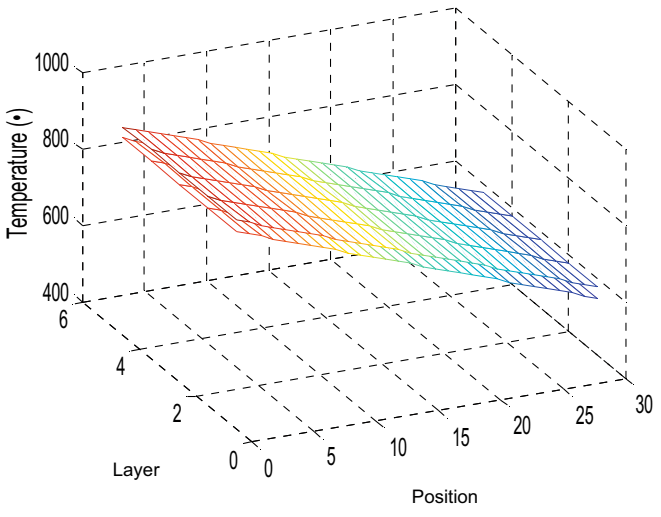

Fig. 6. Initial states of process model and observer.

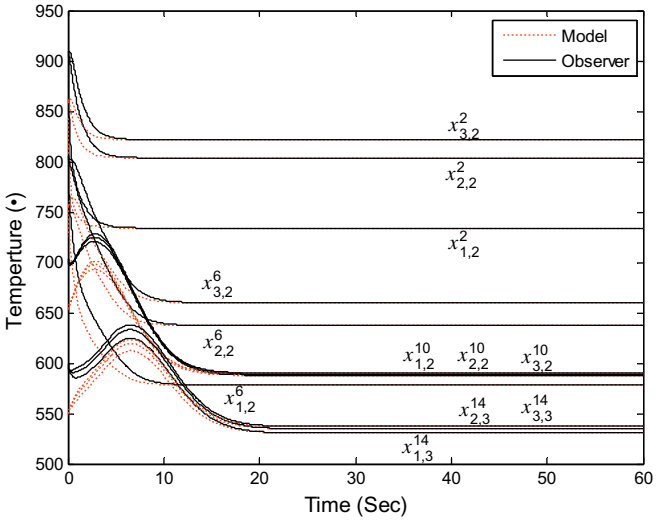

Fig. 7. Comparison of temperatures estimated by process model and observer.

4.3. Performance of DMPC comparing with centralized MPC

Since the main disturbance comes from FT, FT step signal is sent into closed-loop system to compare the performance of the DMPC framework proposed and that of centralized MPC. The thickness of strip equals to 5 mm. Set the prediction horizon $P = 15$, the control horizon $M = 15$ and the control sampling period be 0.37 s.

As shown in Fig. 8, the disturbances coming from FT can be eliminated efficiently through DMPC. Figs. 8 and 9 show that the performance and the manipulated variables of the closed-loop system with DMPC are close to those of centralized MPC when iteration $l \geqslant 3$.

The time cost of centralized MPC and DMPC framework proposed, running in computers with a CPU of 1.8G and a memory of 512M, is illustrated on Table 2. It can be seen that the time consumed by DMPC proposed is quite less than that of centralized MPC. The maximum time cost of DMPC with $l = 3$ is only 0.1192s, which is satisfied with the demand of on-line computation.

4.4. Advantages of the proposed DMPC framework comparing with the existing method

Simulations are performed to illustrate the advantages of the proposed DMPC framework comparing with the existing method

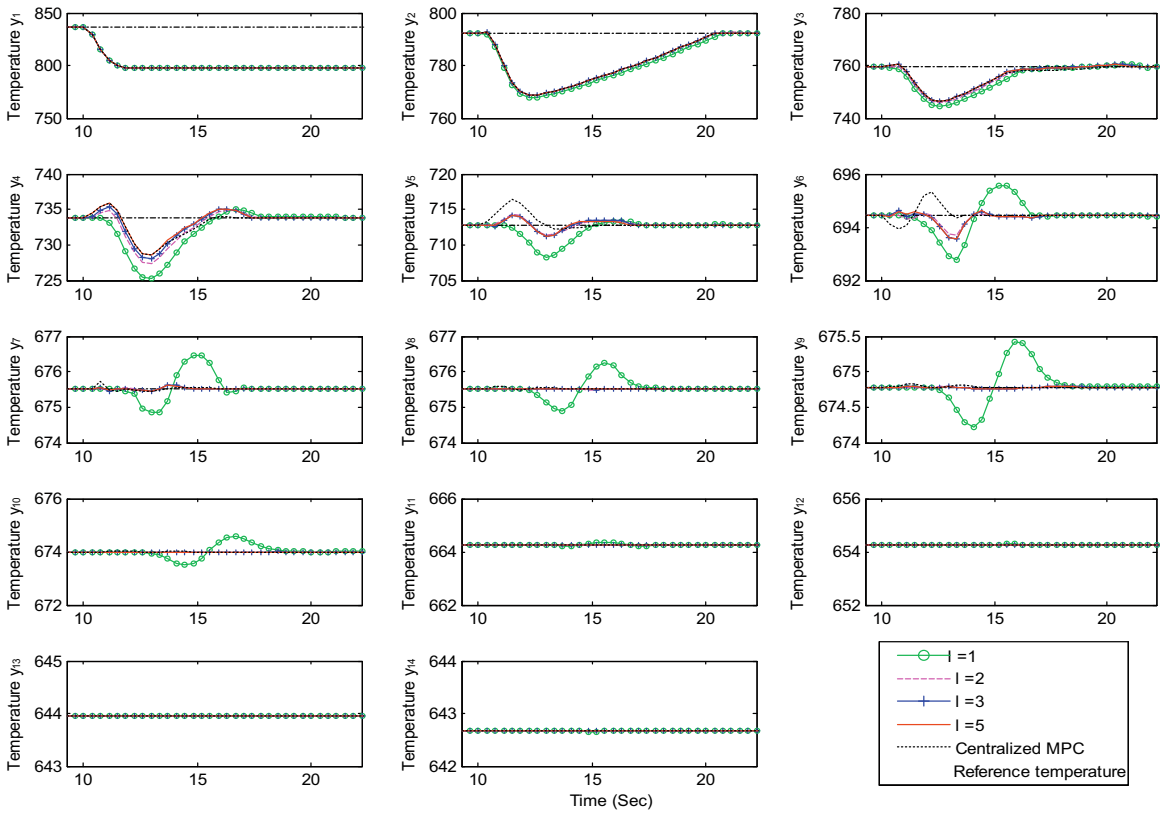

Fig. 8. Performance comparison of different control strategies (centralized MPC and DMPC framework proposed).

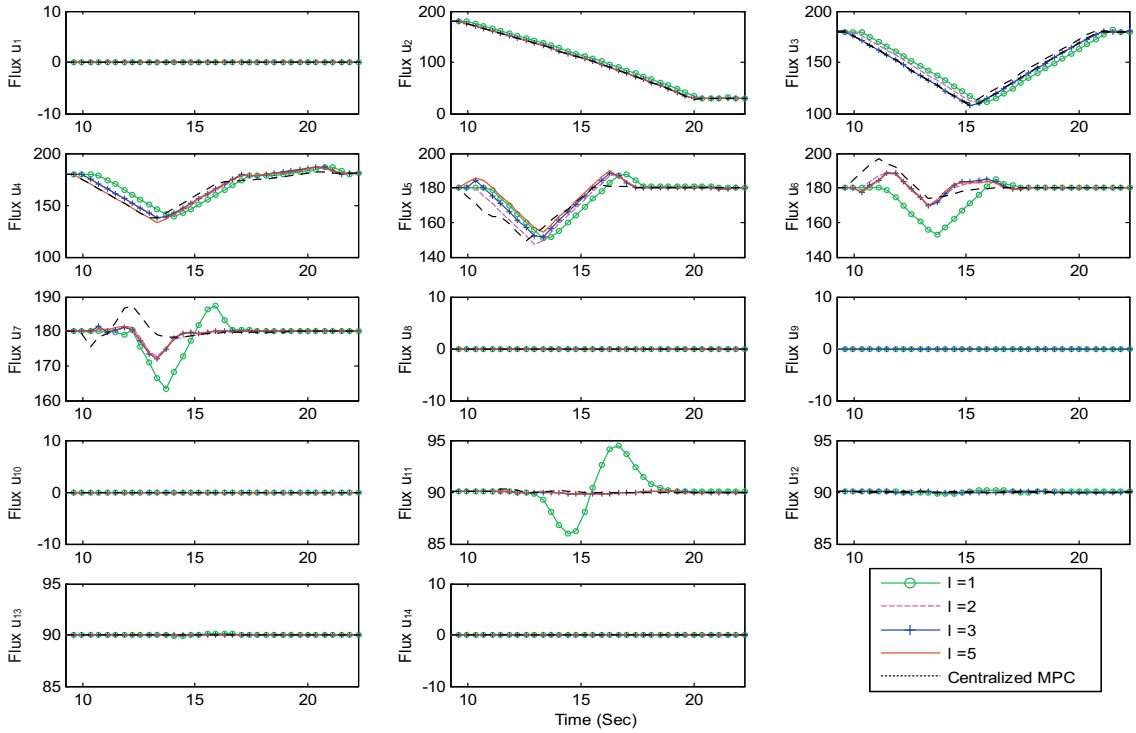

Fig. 9. Flux of each header group with centralized MPC and DMPC framework proposed.

in industrial manufactory. Here, the existing method refers to the open-loop and closed-loop control introduced in Section 2. The cooling curves of each strip-point with the existing method and the proposed DMPC are shown in Figs. 10 and 11, respectively. The existing method is able to control the CT well, while there is a rough approximation of cooling curve for each strip-point

Table 2
Computational burdens of DMPC and centralized MPC.

Item	Minimum time (s)	Maximum time (s)	Average time (s)
Constructing model of each subsystem	0.0008	0.0012	0.0009
DMPC with iteration $l = 1$	0.0153	0.0484	0.0216
DMPC with iteration $l = 2$	0.0268	0.0690	0.0452
DMPC with iteration $l = 3$	0.0497	0.1194	0.0780
DMPC with iteration $l = 5$	0.0895	0.3665	0.1205
Constructing model of overall system	0.0626	0.1871	0.0890
Centralized MPC	0.6535	1.8915	0.9831

Remark: in Table 2, the time cost of constructing system model is included in the time cost of DMPC and centralized MPC.

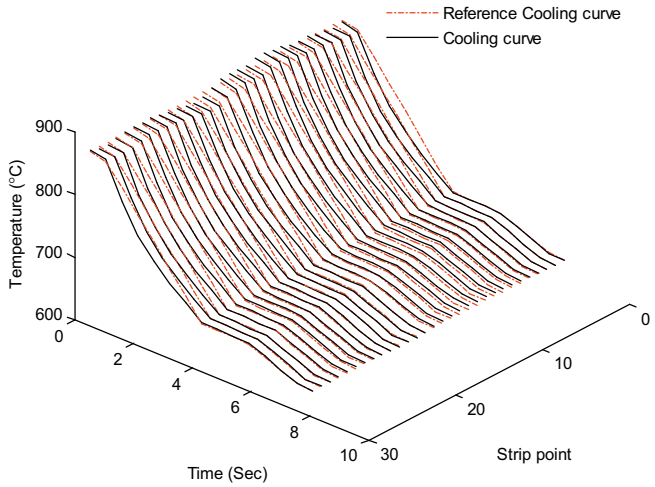

Fig. 10. The cooling curve of each strip-point with existing method.

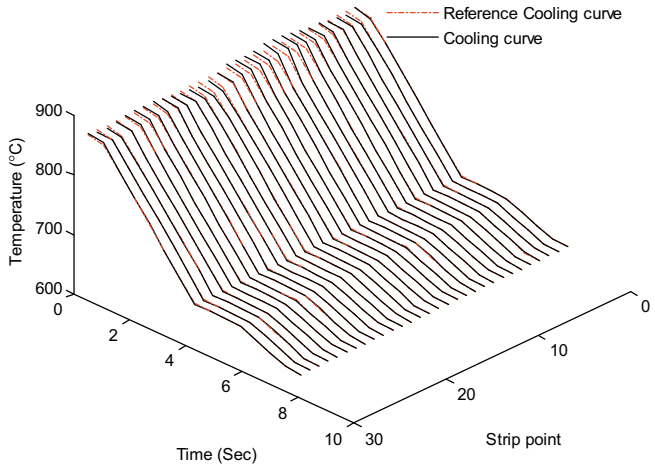

Fig. 11. The cooling curve of each strip-point with DMPC framework proposed.

achieved by the existing method. Typically, the temperatures of strip at the middle of the water cooling section are far away from that of the reference profile. On the contrary, the DMPC is able to adjust the temperature of strip to be consistent with the reference temperature profile at any position of the water cooling section. And a better cooling curve of each strip-point is achieved through it. That means this method is suitable for various cooling curves. And hence the possibility of producing many new types of steel with high quality (e.g. the multi-phase steel) is provided.

4.5. Experimental results

To verify the validation of the method proposed, an experimental result is presented in this subsection. In the experiment, as shown in Fig. 12, the DMPC framework is run in six computers (two for predictors and observer, the other four for local MPCs). The six computers cooperated with each other to derive the optimal inputs within the sampling period of 0.37 s, and then send the optimal inputs into a PLC which charges the field PI controllers. The run-out table experimental apparatus shown in Fig. 13, which is a pilot apparatus, is used to test the performance of the DMPC framework.

The good performance of the proposed DMPC is further verified in Figs. 14–16, which show the FT profile, the output of each closed-loop subsystem and the water flux of each header group

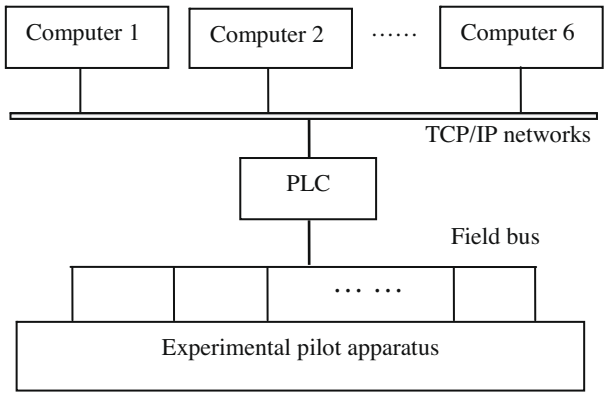

Fig. 12. The structure of experimental system.

Fig. 13. Run-out table pilot apparatus.

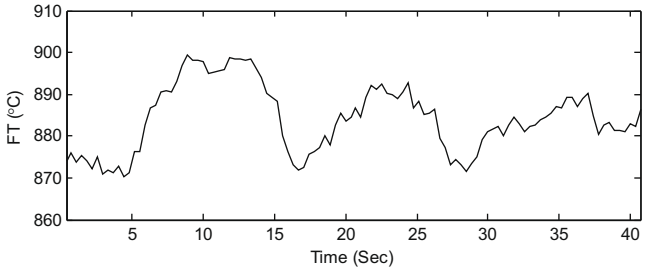

Fig. 14. Finishing rolling temperature of strip.

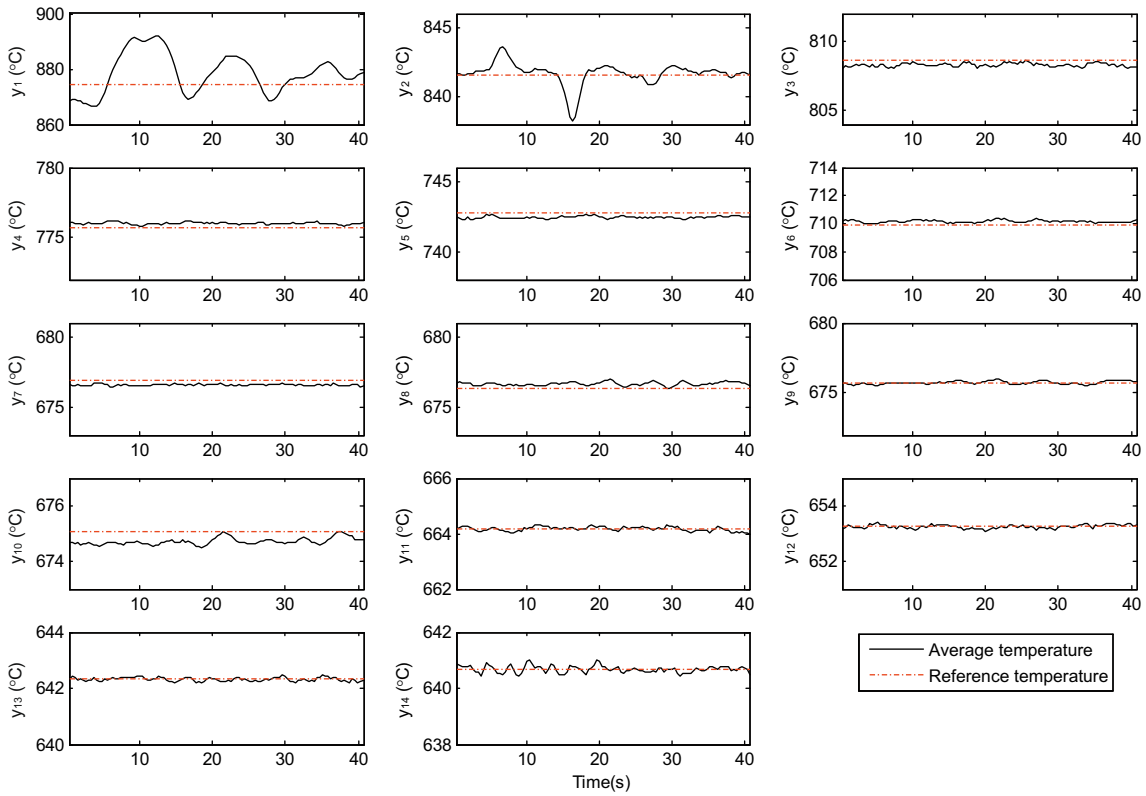

Fig. 15. Output of each closed-loop subsystem with DMPC framework.

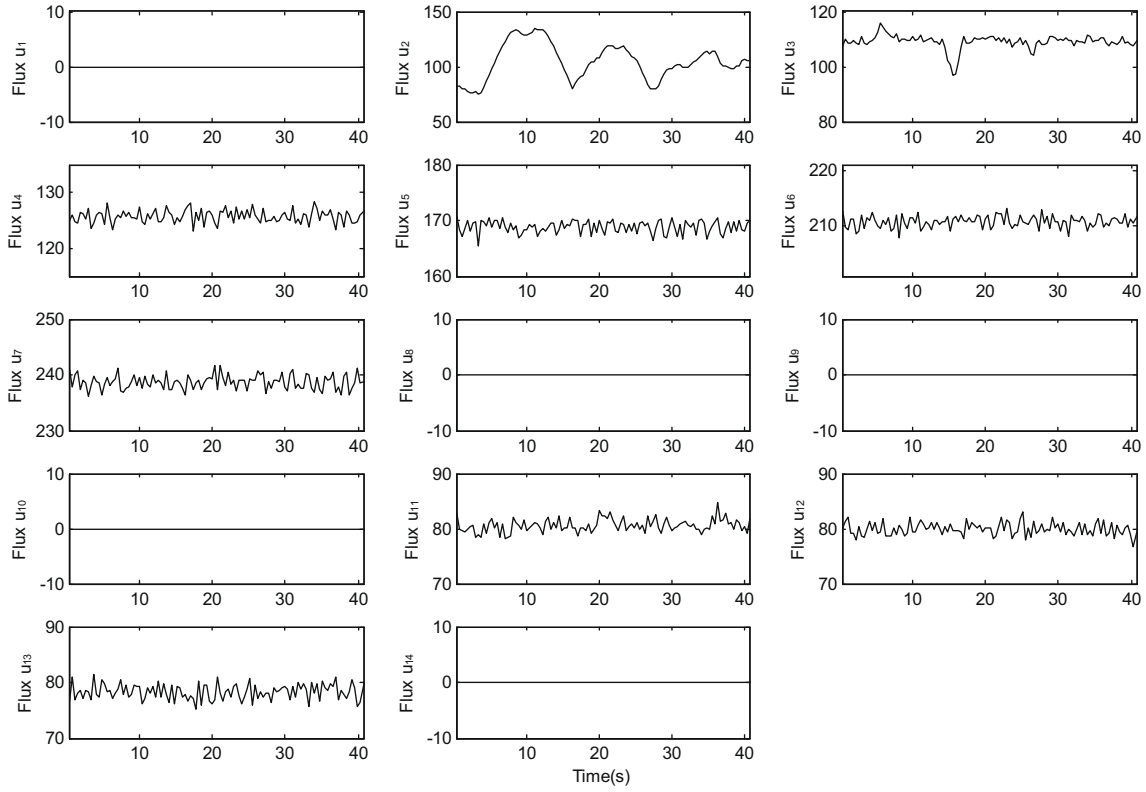

Fig. 16. Flux of each header group with DMPC framework.

in the experiment, respectively. This method can not only control the CT but also optimize the whole evolution of strip temperature online. The flexibility and precision of the control system are enhanced.

5. Conclusions

In the present study, a DMPC framework is designed for the HSLC process, in which the overall system is divided into several interconnected subsystems and each subsystem is controlled by a local MPC. First, the state space representation of each subsystem is developed using finite volume method. Next, an observer based on EKF is designed to reconstruct the current temperature distribution of the strip. Then, the EKF sends current states to the corresponding local MPCs. In each local MPC, neighbourhood optimization is adopted to enhance the global control performance. Furthermore, to overcome the computational obstacle of nonlinear model, the prediction model of each MPC is linearized around the current operating point at each step. Through this method the on-line optimization of strip cooling curve is realized with a few computational burdens, both simulation and experiment results proved the efficiency of the proposed method. Through this method, the whole evolution procedure of strip temperature is controlled online with a relatively high precision, which provides possibilities of producing many new types of steel with high quality (e.g. the multi-phase steel).

In HSLC, the aim is to obtain a uniform microstructure of the strip. Therefore, it is more reasonable that the temperature errors among different strip-points caused by FT are eliminated gradually along the rolling direction. However, in this work, these errors are eliminated mainly by the first several header groups, which is a problem to be solved in further works.

Acknowledgements

This work was supported by the National Nature Science Foundation of China under Grant 60774015, 60825302 and 60674018, the High Technology Research and Development Program of China (Grant: 2006AA04Z173, 2007AA041403), the Specialized Research Fund for the Doctoral Program of Higher Education of China (Grant: 20060248001), and partly by Shanghai Natural Science Foundation (07JC14016). The authors would like to thank the anonymous referees and the editor for their constructive and valuable comments that have improved the presentation.

References

[1] Z.Y. Tang, H. Ding, L.X. Du, H. Ding, X. Zhang, Effect of thermo mechanical processing on microstructures of TRIP steel, Journal of Iron and Steel Research, International 14 (2) (2007) 56–60.
[2] Q.Y. Sha, G.Y. Li, L.F. Qiao, P.Y. Yan, Effect of cooling rate and coiling temperature on precipitate in ferrite of a Nb–V–Ti micro alloyed strip steel, Journal of Iron and Steel Research, International 14 (5) (2007) 316–319.
[3] J. Wang, G.D. Wang, X.H. Liu, Hot strip laminar cooling control model, Journal of Iron and Steel Research International 11 (5) (2004) 13–17.
[4] B. Han, Z.P. Zhang, X.H. Liu, G.D. Wang, Element tracking strategies for hot strip laminar cooling control, Journal of Iron and Steel Research International 12 (3) (2005) 18–21. 27.
[5] H.B. Xie, Z.Y. Jiang, X.H. Liu, G.D. Wang, A.K. Tieu, M. Yang, K. Manabe, Application of fuzzy control of laminar cooling for hot rolled strip, Journal of Materials Processing Technology 187–188 (2007) 715–719.
[6] D.Y. Gong, J.Z. Xu, L.G. Peng, G.D. Wang, X.H. Liu, Self-learning and its application to laminar cooling, model of hot rolled strip, Journal of Iron and Steel Research International 14 (4) (2007) 11–14.
[7] J.M. Maciejowski, Predictive Control with Constraints, Prentice-Hall, London, UK, 2002.
[8] J. Richalet, Industrial applications of model based predictive control, Automatica 29 (1993) 1251–1274.
[9] P.A. Wisnewski, F.J. Doyle, Model-based predictive control studies for a continuous pulp digester, IEEE Transactions on Control Systems Technology 9 (2001) 435–444.
[10] S.J. Qin, T.A. Badgwell, A survey of industrial model predictive control technology, Control Engineering Practice 11 (2003) 733–764.
[11] C. Line, C. Manzie, M.C. Good, Electromechanical brake modeling and control: from PI to MPC, IEEE Transactions on Control Systems Technology 16 (2008) 446–457.
[12] A.G. Wills, D. Bates, A.J. Fleming, B. Ninness, S.O.R. Moheimani, Model predictive control applied to constraint handling in active noise and vibration control, IEEE Transactions on Control Systems Technology 16 (2008) 3–12.
[13] P. Falcone, F. Borrelli, J. Asgari, H.E. Tseng, D. Hrovat, Predictive active steering control for autonomous vehicle systems, IEEE Transactions on Control Systems Technology 15 (2007) 566–580.
[14] S.J. Norquay, A. Palazoglu, J.A. Romagnoli, Application of Wiener model predictive control (WMPC) to an industrial C2-splitter, Journal of Process Control 9 (1999) 461–473.
[15] H. Peng, K. Nakano, H. Shioya, Nonlinear predictive control using neural nets-based local linearization ARX model – stability and industrial application, IEEE Transactions on Control Systems Technology 15 (2007) 130–143.
[16] F. Borrelli, A. Bemporad, M. Fodor, D. Hrovat, An MPC/hybrid system approach to traction control, IEEE Transactions on Control Systems Technology 14 (2006) 541–552.
[17] M. Xu, S.Y. Li, W.J. Cai, Cascade generalized predictive control strategy for boiler drum level, ISA Transactions 44 (2005) 399–411.
[18] W.B. Dunbar, R.M. Murray, Distributed receding horizon control for multi-vehicle formation stabilization, Automatica 42 (2006) 549–558.
[19] T. Keviczky, F. Borrelli, G.J. Balas, Decentralized receding horizon control for large scale dynamically decoupled systems, Automatica 42 (2006) 2105–2115.
[20] W.B. Dunbar, Distributed receding horizon control of dynamically coupled nonlinear systems, IEEE Transaction on Automatic Control 52 (2007) 1249–1263.
[21] E. Camponogara, D. Jia, B.H. Krogh, S. Talukdar, Distributed model predictive control, IEEE Transaction on Control Systems Magazine 9 (2002) 44–52.
[22] S.Y. Li, Y. Zhang, Q.M. Zhu, Nash-optimization enhanced distributed model predictive control applied to the Shell benchmark problem, Information Sciences 170 (2005) 329–349.
[23] A.N. Venkat, J.B. Rawlings, S.J. Wright, Distributed model predictive control of large-scale systems, in: Assessment and Future Directions of Nonlinear Model Predictive Control, Springer, Berlin Heidelberg, 2007, pp. 591–605.
[24] Y. Zhang, S.Y. Li, Networked model predictive control based on neighbourhood optimization for serially connected large-scale processes, Journal of Process Control 17 (2007) 37–50.
[25] A.N. Venkat, I.A. Hiskens, J.B. Rawlings, S.J. Wright, Distributed MPC strategies with application to power system automatic generation control, IEEE Transactions on Control Systems Technology 16 (2008) 1192–1206.
[26] S. Latzel, Advanced automation concept of run-out table strip cooling for hot strip and plate mills, IEEE Transaction on Industry Applications 27 (2001) 1088–1097.
[27] R.D. Pehlke, A. Jeyerajan, H. Wada, Summary of Thermal Properties for Casting Alloys and Mold, Materials, Department Materials and Metallurgical Engineering, University of Michigan, Ann Arbor, 1982.
[28] Hans Baehr, Heat and Mass Transfer, Springer, Berlin Heidelberg, 2006.
[29] M. Boutayeb, H. Rafaralahy, M. Darouach, Convergence analysis of the extended Kalman filter used as an observer for nonlinear deterministic discrete-time systems, IEEE Transactions on Automatic Control 42 (1997) 581–586.
[30] M.R. Katebi, M.A. Johnson, Predictive control design for large-scale systems, Automatica 33 (1997) 421–425.
[31] L. Chisci, P. Falugi, G. Zappa, Gain-scheduling MPC of nonlinear systems, International Journal of Robust Nonlinear Control 13 (2003) 295–308.
[32] Z. Wan, M.V. Kothare, Efficient scheduled stabilizing model predictive control for constrained nonlinear systems, International Journal of Robust Nonlinear Control 13 (2003) 331–346.
[33] T. Keviczky, G.J. Balas, Flight test of a receding horizon controller for autonomous UAV guidance, in: Proceedings of the American Control Conference, 2005, p. 3518–3523.
[34] N. Blet, D. Megias, J. Serrano, C. de Prada, Nonlinear MPC versus MPC using on-line linearization – a comparative study, in: IFAC World Congress, B'02, Barcelona, Spain, 2002.